CALCULATING THE ROLLING RESISTANCE DIRECTLY FROM THE KINEMATICS AND HANDRIM-FORCES OF THE WHEELCHAIR USER DURING MANUAL WHEELCHAIR PROPULSION USING AN INVERSE DYNAMICS SIMULATION MODEL

Robert Rooijmans
Student TU Delft
Student ID: 4362586

December 8, 2021

Master of Science Thesis
BioMechanical Design: BioRobotics
Supervisors:
Prof. Dr. DirkJan Veeger & PhD Researcher Marit van Dijk

Acknowledgements

Without the help and expertise of prof. dr. DirkJan Veeger and Ph.D. researcher Marit van Dijk the completion of this master thesis would not have been possible, so I would like to express my sincerest thanks to them. Although times have been challenging during the COVID-19 pandemic, their guidance and feedback kept me motivated to complete this research. With the abundance of knowledge and experience in the field of wheelchair biomechanics, H.E.J. Veeger was always able to answer my questions and point me in the right direction when I got stuck during my research. Furthermore, Marit van Dijk was always able to help me progress this study with her intelligent and enthusiastic view on the problems that I faced during my master thesis.

Additionally, I would like to express my gratitude to my girlfriend Yarden, parents Coen and Juliette, and brothers Bart en Joost for their unconditional love and support during my student days. A special thanks also to my old roommates at the Raamstraat in Delft and current roommates in Rotterdam for the interesting discussions and unforgettable times we experienced together during my student days.

Context of this Master Thesis: Project WheelPower

Improving the performance of wheelchair athletes through technology and data shows great promise. In this context Project WheelPower was founded (*WheelPower*, 2021). This Dutch research consortium, consisting of several universities and sports institutions, aims to improve the performance of wheelchair athletes using scientific methods. Having recognized the significance of rolling resistance in wheelchair sports and the lack of dynamical models available in scientific literature to accurately describe the causes of this rolling resistance, this master thesis was initiated at the TU Delft.

Contents

ABSTRACT

The main resistive force acting on the wheelchair during manual wheelchair propulsion is the rolling resistance. The magnitude of this rolling resistance is heavily influenced by the actions of the wheelchair user. By optimizing how wheelchair athletes move, this rolling resistance can be minimized, thereby improving their effective power output. However, in scientific literature, there are no dynamic models that analyze the direct effect of the wheelchair user's actions on the rolling resistance. To fill this research gap, this master thesis was initiated. In this master thesis, a simulation model is created that can calculate the rolling resistance directly from the wheelchair user's actions. This inverse dynamic model was created by combining a dynamical model that calculates the rolling resistance with a segmented model of the wheelchair user. To test this simulation model data were gathered using coasting tests and manual wheelchair propulsion tests. The first results were promising. The results of the calculated rolling resistance seemed plausible and the effect of the wheelchair user's actions was clearly visible. This makes this simulation model a useful tool to analyze the effect of the wheelchair user's actions on the rolling resistance. The most important factor in determining the magnitude of the rolling resistance appeared to be the thorax angle. This is in accordance with scientific literature, as leaning forwards shifts the weight distribution forwards. Multiple studies show that shifting the weight distribution forwards causes a significant increase in the magnitude of the rolling resistance. Further research to confirm the validity of this simulation model is still required.

1 Introduction

Sports nowadays are becoming more and more driven by technology and data. Paralympic sports are no different in this aspect. Studies show that propulsion technique can have an impact on the mechanical efficiency of wheelchair users. Research by De Groot et al. indicated that three weeks of practice already affected technique variables such as push time and push frequency. Furthermore, a significant improvement in mechanical efficiency during manual wheelchair propulsion could be identified after three weeks of practice (De, Veeger, Hollander, & der Woude Van, 2002). This indicates that studying the relationship between the propulsion technique and the mechanical efficiency during manual wheelchair propulsion could be a useful tool to improve their performance.

Furthermore, the movement of the wheelchair user is an important factor in the magnitude of the rolling resistance force acting on the wheelchair (Vanlandewijck, Theisen, & Daly, 2001). The primary cause of rolling resistance is deformation of the tires, which results in energy losses due to hysteresis. When talking about rolling resistance in this paper, only this cause of rolling resistance is considered. So effects on the rolling resistance due to inelastic deformation, surface roughness and slipping of the tire are not included in the simulation model used in this paper (Kauzlarich & Thacker, 1985). If the movement of the wheelchair user causes the weight distribution acting on the wheelchair to shift forwards, the load on the caster wheels increases. The caster wheels have a significantly smaller radius than the rear wheels. This means that the tire deformation of the caster wheels is also proportionally greater than the tire deformation of the rear wheels during wheelchair propulsion. From this, it follows that shifting the weight distribution forwards leads to an increase in rolling resistance. As wheelchair athletes want to minimize this rolling resistance,

quantifying exactly how the actions of the wheelchair user impact the rolling resistance can give useful insights for improving the performance of these wheelchair athletes. However, this is where most dynamic models of wheelchair propulsion currently available in scientific literature are lacking. Most dynamical models focus mainly on the wheelchair user OR on the dynamics and rolling resistance of the wheelchair itself instead of a combination of these two.

So why can most dynamical models of wheelchair propulsion not be used to study the direct effect of the wheelchair user's actions on rolling resistance? This can be explained by the fact that the research in the field of wheelchair biomechanics is often focused on the pathology of wheelchair users. Multiple examples of dynamical models that can be used for this purpose can be found in literature. Many cases of 2-dimensional (Morrow, Guo, Zhao, Su, & An, 2003; Leary et al., 2012; de Barros Lombardi Jr & Dedini, 2009) and 3-dimensional dynamical models (Veeger, Van Der Woude, & Rozendal, 1991; Desroches et al., 2010; Rodgers, Tummarakota, & Lieh, 1998) exist to study the load on (shoulder) joints and body segments. Some dynamical models that can be used to study the biomechanics of wheelchair propulsion even include muscle models to estimate the strain on specific muscles during manual wheelchair propulsion. Most notable contributions in this specific field are made by the Delft elbow and shoulder model (DESM) (Van der Helm, 1994; Nikooyan, Veeger, Chadwick, Praagman, & van der Helm, 2011), the Swedish shoulder (SSM) model (Högfors, Sigholm, & Herberts, 1987; Karlsson & Peterson, 1992) and the Newcastle or UK national shoulder model (UKNSM) (Charlton & Johnson, 2006). As these models are mostly focused on the load on the joints and muscles, wheelchair dynamics are often omitted in these dynamic models.

However, there are examples of dynamical models in scientific literature that study rolling resistance during manual wheelchair propulsion. Yet most of these models seldom calculate the rolling resistance directly from the kinematics and kinetics of the wheelchair and wheelchair user. Using coasting tests, the rolling resistance of the wheelchair can easily be quantified. During these coast-down tests, the deceleration of the center of mass of the wheelchair is measured. Because air resistance during wheelchair propulsion at low speeds (< 20 km / h) (Warguła, Wieczorek, & Kukla, 2019) and the internal friction (Bascou, Sauret, Lavaste, & Pillet, 2017) can be neglected, the rolling resistance can be estimated from this deceleration. For example, Sauret et al. (Sauret et al., 2012) constructed a dynamical model to determine the rolling resistance parameters. By equating the deceleration of the wheelchair to the calculated rolling resistance generated by the normal forces acting on the front and rear wheels, the rolling resistance parameters can be estimated. However, this research used fixed mass distributions on front and rear wheels using weights. Therefore it does not account for the actions of the wheelchair user. Furthermore, the rolling resistance is estimated from the deceleration of the wheelchair instead of calculating it directly from the normal forces acting on the front and rear wheels. Dynamical models of wheelchair propulsion that are not subject to both these limitations are lacking in scientific literature. A later dynamical model by Sauret et al. comes closer in this regard (Sauret, Vaslin, Lavaste, de Saint Remy, & Cid, 2013). This dynamical model does calculate the rolling resistance from the normal forces acting on the front and rear wheels and also uses the applied forces by the wheelchair user as an input. However, these applied forces by the wheelchair user are measured and not calculated from the kinematics of the body segments of the wheelchair user. This might limit the insights into the direct effect of the wheelchair user's actions and the calculated rolling resistance.

1.1 Research goal

As previously mentioned, studying the direct effect of the wheelchair user's actions on the rolling resistance could be a useful tool for wheelchair athletes. Namely, if this effect is better understood, wheelchair athletes could use this knowledge to minimize the rolling resistance and thereby improve their performance during manual wheelchair propulsion. To fill the research gap apparent in this field a new dynamic model is constructed in this research. This model is a combination of the dynamic model of the wheelchair by Sauret et al. (Sauret et al., 2013) and a segmented model of the wheelchair user based on the model by Leenen and van Trigt et al. (Leenen, Trigt, Hoozemans, & Veeger, 2020). To directly calculate the normal forces and herewith the accompanying rolling resistance during manual wheelchair propulsion, Sauret et al. constructed a dynamical model of the wheelchair (Sauret et al., 2013). This dynamical model can be seen in figure 1 below.

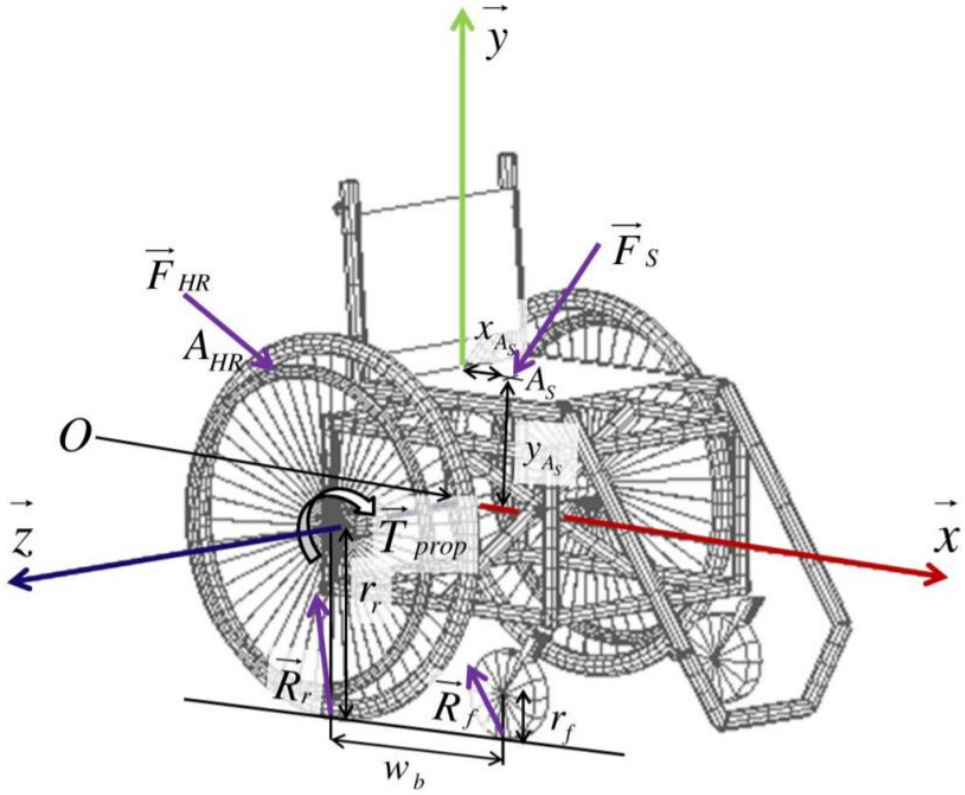

Figure 1: Dynamical model of the wheelchair to calculate normal forces acting on the front and rear wheels (Sauret et al., 2013)

In this model, the normal forces of the front and rear wheels are calculated as a result of the handrim forces and the forces and torques that the wheelchair user applies to the wheelchair. Using dynamo-meters between the seat and the frame and on the handrim, data were gathered on the applied forces and torques to validate this model. When working with wheelchair athletes, such a set-up to acquire this data is not always desirable or even not possible. Furthermore, this direct measurement of applied forces and torques on the wheelchair as input data might limit the insights into the relationship between the wheelchair user's actions and the rolling resistance. By calculating these applied forces and torques on the wheelchair directly from the kinematics of the wheelchair user, the causality between the wheelchair user's action and rolling resistance can become more

apparent. Therefore, in this research, the forces and torques that are applied to the wheelchair are calculated directly from the kinematics of the wheelchair user. These kinematics can, for example, be tracked using Inertial Measurement Units (see chapter 4.1) using a relatively simple experimental set-up. Using this kinematic data together with data on the applied handrim forces, the rolling resistance can then be calculated directly from the actions of the wheelchair user. By combining the segmented model of the wheelchair user with the dynamical model of Sauret et al. the relationship between the wheelchair user's actions and the generated rolling resistance can then be analyzed. This leads to the following research question of this master thesis.

Research question:

*How can the **rolling resistance** be calculated directly from the wheelchair user's **kinematics** and **handrim forces** during manual wheelchair propulsion using a segmented inverse kinematic model?*

To answer this research question, this report is divided into several chapters. Firstly, some theoretical background is expanded on in chapter 2. After this, the construction of the simulation model in python is explained in chapter 3. To validate this simulation model, experimental data is required. The collection and processing of these data are discussed in chapter 4. Using these experimental data, the simulation model is tested. After this, the results of this model are outlined in chapter 5 and subsequently discussed in chapter 6. Lastly, the conclusions and recommendations will be made in chapter 7.

2 Theoretical Background

This chapter presents the theoretical framework of this master thesis. To explain the workings of the simulation model used in this research, some theoretical background is required. Firstly, a short introduction of inverse dynamics is given in chapter 2.1. After this, the method to calculate the rolling resistance acting on the wheelchair is expanded on in chapter 2.2.

2.1 Inverse dynamics models

Most dynamical models that investigate the biomechanics of wheelchair propulsion make use of inverse dynamics models. Inverse dynamics is a method to calculate the forces and torques using kinematics as input. As during wheelchair propulsion the joint loads and moments can not be measured in vivo, inverse dynamics is often the only solution to gain insights into the biomechanics of wheelchair propulsion. Inverse dynamics uses the kinematics, external forces, and the body's inertial properties such as mass and moment of inertia as an input to calculate the internal forces and moments. The dynamical model used in this research makes use of the Newton-Euler equations listed below in formulas 1 and 2 to calculate the internal forces and torques of the system.

$$F = m * a \tag{1}$$

$$T = I * \omega \tag{2}$$

2.2 Rolling resistance

The main goal of this research is to calculate the rolling resistance directly from the kinematics of the wheelchair and wheelchair user. The rolling resistance is a resistive force acting on a moving body when it rolls on a surface. This is mainly due to deformation of the tires. As the wheel rolls on the surface, it deforms when pressure is exerted on the wheels. Not all of the energy that needed to achieve this deformation is recovered when the pressure is released and the wheel returns to its original form, resulting in the resistive force we call rolling resistance. A simplified formula to calculate this rolling resistance can be seen in formula 3 below:

$$F_{roll} = C_{rr} * N \tag{3}$$

In this equation, C_{rr} is the rolling coefficient. This dimensionless coefficient is dependable on multiple factors such as material properties, wheel diameter, speed, and many others. N denotes the normal forces of the ground acting on the tires. To calculate the total rolling resistance acting on the wheelchair, equation 4 listed below can be used:

$$F_{roll} = -(\frac{\lambda_f}{r_f} N_f + \frac{\lambda_r}{r_r} N_r) \tag{4}$$

In this equation, the rolling resistance of the front and rear tires are calculated separately as they have different radii and rolling resistance parameters r and λ. However, since this research focuses on straight-line wheelchair propulsion, the load on both the rear wheels is assumed to be equally distributed as is the load on the front wheels. Now only the normal forces N acting on the front

and rear tires need to be considered. It is important to note that these normal forces do not simply equal the gravitational force of the wheelchair and the wheelchair user. The upper body of the wheelchair user usually moves a lot during manual wheelchair propulsion. The acceleration of the center of mass of the wheelchair user in the vertical direction can increase or decrease the load that the wheelchair user exerts on the wheelchair in accordance with equation 1. Furthermore, the kinematics of the upper body can result in significant shifts in the weight distribution acting on the rear and front wheels. This is clearly demonstrated in research by Sauret et al., where the calculated normal forces acting on the rear and front wheels varied over wide ranges during the propulsion cycle. The measured load on the front wheels expressed as a percentage of the total load varied from 30% to over 60% (Sauret et al., 2013).

To calculate these normal forces the dynamical model of Sauret et al. (Sauret et al., 2013) is used that can be seen in figure 1. The equation for the normal force acting on the rear tire follows from the balance of forces in the vertical direction as can be seen in equation 5. As the center of mass of the wheelchair is assumed not to move in the vertical direction, the sum of the vertical force components equals zero.

$$Wwc + F_{sy} + F_{HRy} + N_f + N_r = 0 \tag{5}$$

In this equation, W_{wc} equals the weight of the wheelchair and lower body of the wheelchair user, F_{sy} is the vertical force that the wheelchair user applies on the seat of the wheelchair (including gravitational forces) and F_{HRy} is the handrim force applied by the wheelchair user in the vertical direction. From this equation, the normal force on the rear tire can be expressed as in equation 6.

$$N_r = -(Wwc + F_{sy} + F_{HRy} + N_f) \tag{6}$$

Now only an expression of the normal force acting on the front wheels is needed. This expression follows from the sum of external moments acting on the center of the rear wheels. A simplified form of this equation results in the expression for the normal force acting on the front wheels as can be seen in equation 7 (Sauret et al., 2013).

$$N_f = -\frac{(x_{As}F_{sy} - yAsF_{sx} + Tsz) + x_G Wwc}{w_b} \tag{7}$$

In this equation, x_{As} equals the fore-aft distance from the center of mass of the wheelchair to the point of application of the force applied by the wheelchair user on the seat. y_{As} is the vertical distance between these two points. T_{sz} is the torque that the wheelchair user applies on the seat of the wheelchair, x_G is the fore-aft distance between the rear wheel axle and the center of mass of the wheelchair and w_b is the wheelbase (fore-aft distance between the rear and front wheel axle) of the wheelchair.

Combining equation 4 for rolling resistance with equations 6 and 7 for the normal forces acting on the rear and front wheels gives the following expression for the total rolling resistance acting on the wheelchair in equation 8:

$$F_{rolltotal} = -(\frac{\lambda_f}{r_f}\frac{(x_{As}F_{sy} - yAsF_{sx} + Tsz) + x_G Wwc}{w_b} + \frac{\lambda_r}{r_r}(-(Wwc + F_{sy} + F_{HRy} + N_f))) \tag{8}$$

3 Python Segmented Simulation Model

To investigate how the actions of the wheelchair user directly impact the rolling resistance acting on the wheelchair, a simulation model needs to be constructed. This model is based on the segmented model used by Leenen and van Trigt et al. (Leenen et al., 2020) and the model to calculate the rolling resistance acting on a wheelchair by Sauret et al. (Sauret et al., 2013). The model of Leenen et al. has been used to analyze the biomechanics of baseball pitching, but can be adapted for other purposes as well. The model is constructed in Python (PYTHON, 2021) and makes use of several python packages (Harris et al., 2020; Hunter, 2007; Virtanen et al., 2020; pandas-development team, 2020). Firstly, in chapter 3.1, the model constructed by Leenen and van Trigt et al. will be introduced, which is defined as the unadapted segmented simulation model. To use this model for analyzing the biomechanics of wheelchair propulsion and implement the dynamical model of Sauret et al. to calculate the rolling resistance, some adaptations to the model have to be made. In chapter 3.2 these adaptations are further expanded on. Lastly, some assumptions and simplifications made in the construction of this simulation model are discussed in chapter 3.3.

3.1 Unadapted Segmented Simulation Model

The unadapted model by Leenen et al., which is used to analyze baseball pitching, is an inverse-kinematic model. As explained in chapter 2.1, this means it uses measured kinematics of the body segments to calculate the internal forces and moments acting on the segment joints. As of 2021, the model includes the following segments: hand, forearm, upper-arm, thorax and pelvis.

Using kinematic data from markers on bony landmarks it calculates the local coordinate system of the separate segments at all time steps according to the ISB-definition (Wu et al., 2002, 2005). To calculate the local coordinate system of the different segments, the following bony landmarks are used per segment: for the thorax bony landmarks IJ, PX, C7 and T8, for the pelvis bony landmarks RSIAS, LSIAS, RSIPS and LSIPS, for the upper arm LHE, MHE and AC, for the forearm LHE, MHE, US and RS and finally for the hand US, RS and MH3. The center of mass location and inertial tensors for all the segments are calculated using the regression equations by Zatsiorsky (Zatsiorky, 1990).

3.1.1 Unadapted Segmented Simulation Model: Net Force Calculation

After the kinematic data and inertial properties of the included segments have been defined, first, the net forces acting on the segments using inverse dynamics are calculated. This calculation can either be performed top-down or bottom-up. For example, in a top-down model including the hands, forearms, upper-arms and thorax, the internal forces are calculated for the separate segments in the order in which they are listed here. Starting with the hands, the internal forces are calculated using the newton equations of motion mentioned in chapter 2.1. For the hand, in this case, no force from the most distant segment can act on the hand since the hand itself is the most distant segment. This results in equation 9 that can be rewritten to equation 10 to calculate the proximal joint (wrist) force acting on the hand:

$$m_{seg}a = \sum F = F_{prox} + m_{seg}g \tag{9}$$

$$F_{prox} = m_{seg}a - m_{seg}g \tag{10}$$

Then for the next segment, in this case the forearm, the distal force equals minus the proximal force from the previous segment. This is due to Newton's third law: $action = -reaction$. For the subsequent segments the proximal forces acting on the concerned segments can then be calculated using equation 11 below:

$$F_{prox} = m_{seg}a - m_{seg}g - F_{dist} \tag{11}$$

3.1.2 Unadapted Segmented Simulation Model: Net Moment Calculation

After all the internal forces have been determined, the internal moments can be calculated using the Newton-Euler equations explained in chapter 2.1. For every segment the proximal moment acting on the concerned segment is calculated using equations 12 and 13 listed below:

$$M_{prox} = MI - MF_{prox} - MF_{dist} - M_{dist} \tag{12}$$

with

$$MI = I\alpha + \omega \times I\omega \tag{13}$$

In equation 12, MF_{prox} is the moment that is generated by the forces acting on the proximal joint and MF_{dist} is the moment that is generated by forces acting on the distal joint. M_{dist} is the moment exerted by the distal joint. In equation 13, I is the moment of inertia matrix, α the angular acceleration and ω the angular velocity.

For example, in a top-down model including the hands, forearms, upper-arms and thorax, the distal moments and moments generated by distal forces acting on the hand are equal to zero. Then again using Newton's third law of $action = -reaction$, when setting up the moments balance for the next segment, in this case the forearm, the distal moment is equal to minus the proximal moment acting on the hand.

3.2 Adapted Segmented Simulation Model

When using this model to analyze wheelchair biomechanics, some adaptations need to be made to the simulation model. For simplicity purposes, only three of the possible segments are included in the simulation model of the wheelchair and the wheelchair user: the forearm, upper-arm and thorax. However, a fourth "segment" was added to the simulation model, namely the wheelchair including the lower body of the wheelchair user. As the wheelchair user is assumed to not move its lower body relative to the wheelchair, it can be assumed to be part of one segment.

3.2.1 Adapted Segmented Simulation Model: Net Force Calculation

Also regarding the net reaction forces calculations, some changes are required. During manual wheelchair propulsion, an external force acts on the wheelchair user as a result of pushing the handrim. This force should be added to the force balance of the first segment of this model, namely the forearm. This can be seen in equation 14.

$$F_{prox} = m_{seg}a - m_{seg}g - F_{ext} \tag{14}$$

The force balance of the wheelchair segment is of course different from the other segments that are included in the model. It requires the addition of three force components: the effective propulsion force, the rolling resistance force and the handrim force. The resulting equation 15 can be seen below:

$$F_{prox} = m_{seg}a - m_{seg}g - F_{dist} - F_{propulsion} - F_{roll} - F_{handrim} \tag{15}$$

Note that the propulsion force does not equal the handrim force in the fore-aft direction, as not all the generated force in this direction is effectively propelling the wheelchair forwards. If the wheelchair user exerts a handrim force in the forward direction at the "three o'clock" point of the handrim, the wheelchair will not move forwards as the body of the wheelchair user pushes back the wheelchair with an equal force. This force would not create a torque about the rear wheel axle. Only the force components acting on the handrim that generate a torque about the rear wheel axle result in an effective propulsion force. This propulsion force can be determined by dividing the moment acting on the rear wheel axle by the radius of the rear wheel, as can be seen in equation 16:

$$F_{propulsion} = \frac{T_{wheelaxle}}{r_{rear}} \tag{16}$$

The rolling resistance equations from Sauret et al. (Sauret et al., 2013) are used to determine the rolling resistance force as they are explained in section 2.2. However, in this case, the forces acting on the seat are not measured using dynamometers but are instead calculated from the kinematics of the wheelchair user. This will come with its difficulties, as x_{As} and y_{As} from equation 7 can no longer be determined using simple measurements. More on this in chapter 3.3. Furthermore, the torque exerted by the wheelchair user on the seat is not measured anymore but follows from the net moment calculations of the other segments.

3.2.2 Adapted Segmented Simulation Model: Net Moment Calculation

The external forces and moments also influence the moment equation for the forearm segment as can be seen in equation 17. M_{ext} is the external moment acting on the segment and MF_{ext} is the moment that is generated by the external forces acting on the segment. In the case of this dynamical model of the wheelchair and wheelchair user, these external forces and moments are created by the reaction of the handrim forces and moments acting on the forearm.

$$M_{prox} = MI - MF_{prox} - MF_{dist} - M_{dist} - MF_{ext} - M_{ext} \tag{17}$$

3.2.3 Adapted Segmented Simulation Model: the Free Body Diagram

To visualize the dynamics of the complete wheelchair and wheelchair user system, a free-body diagram was constructed. This free body diagram, including the equations of motion, can be seen in figure 2.

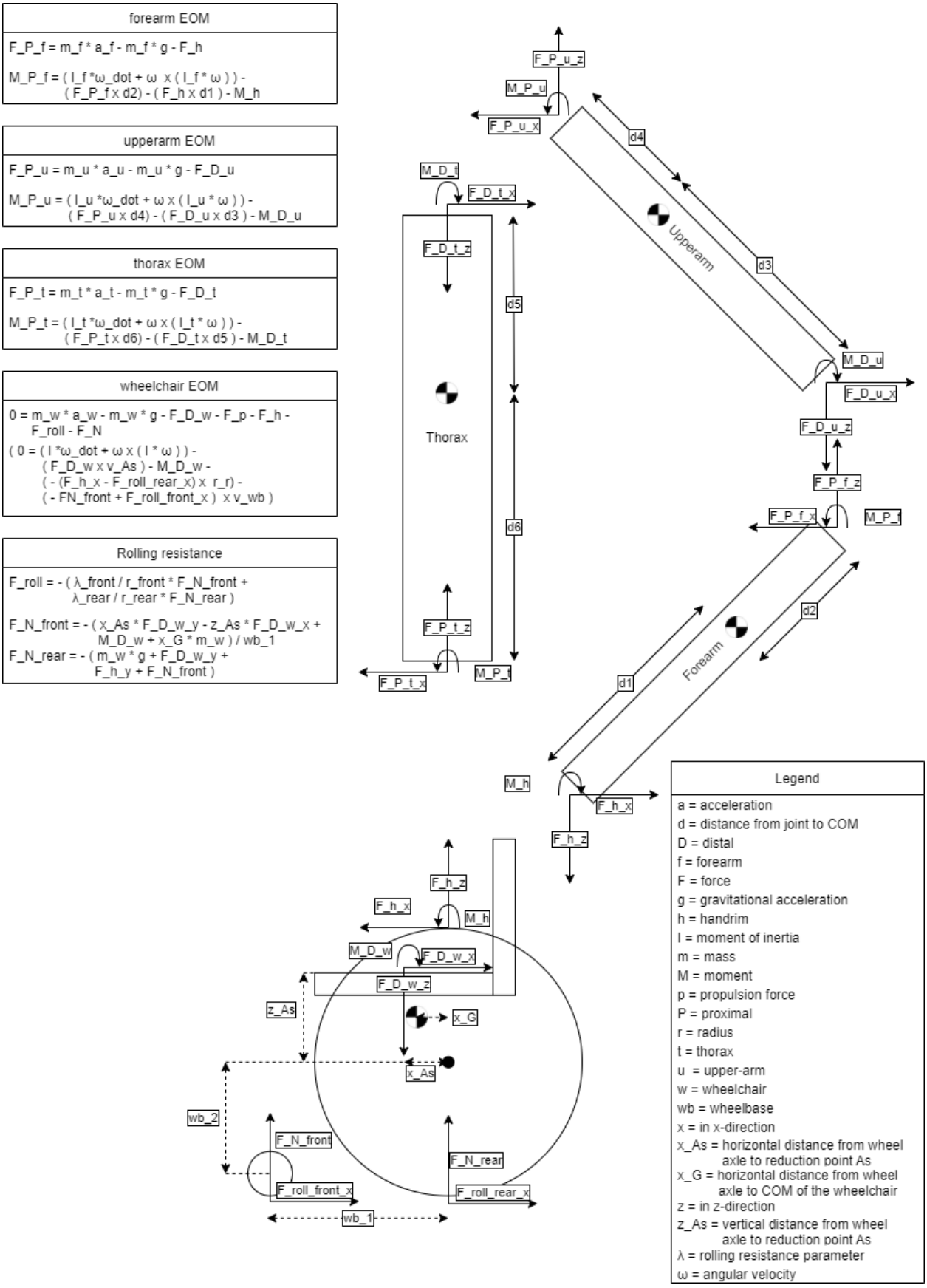

Figure 2: The free body diagram of the wheelchair and wheelchair user system

3.3 Assumptions and Simplifications

To better interpret the working and results of this simulation model, it is important to understand what assumptions and simplifications have been made in the construction and use of this simulation model during this research. In this chapter, the most important assumptions and simplifications are briefly explained. Firstly, the method to calculate the acceleration of the center of mass of the thorax is described. After this, the addition of the arms to the dynamical model is outlined. Lastly, the use of the reduction point and quantification of some input parameters are explained.

3.3.1 Estimating the Acceleration of the Center of Mass of the Thorax

One of the inputs of the simulation model of the wheelchair and wheelchair user is the acceleration of the center of mass of the thorax. The acceleration of the center of mass of the thorax is approximated using the data from the gyroscope of the NGIMU (see section 4.1) strapped on the sternum of the test subject. The gyroscope measures the angular velocity, which is filtered and differentiated to acquire the angular acceleration of the thorax. Using anthropometric measurements, the distance from the hip bone to the center of mass of the thorax is estimated. If the thorax is then assumed to be a stiff rod, the acceleration of the thorax can be calculated. However, this simplification leads to significant errors in the estimation of this acceleration, as the lower end of the thorax often stays still while the upper end of the thorax bends forwards. To prevent the overestimation of the thorax center of mass acceleration, the length of the "rod" that represents the thorax is reduced by a factor. To verify the magnitude of this factor, data from the Optotrack system are compared with data from the NGIMU's from the treadmill experiments. The acceleration of the center of mass of the thorax is estimated with NGIMU's using the aforementioned method and with a factor of 0.45. The Optotrack system measures the position of four bony landmarks on the thorax: incisura jugularis sternalis (1), processus xiphoideus (2), processus spinosus of cervical vertebrae 7 (3) and processus spinosus of thoracic vertebrae (4). From these four bony landmarks, the center of mass location of the thorax is estimated. By differentiating this data twice, the acceleration of the center of mass is determined. A comparison between the two different methods to estimate the acceleration can be seen in figure 3 below. Although some differences are apparent, both methods yield relatively similar estimations of the acceleration of the center of mass of the thorax.

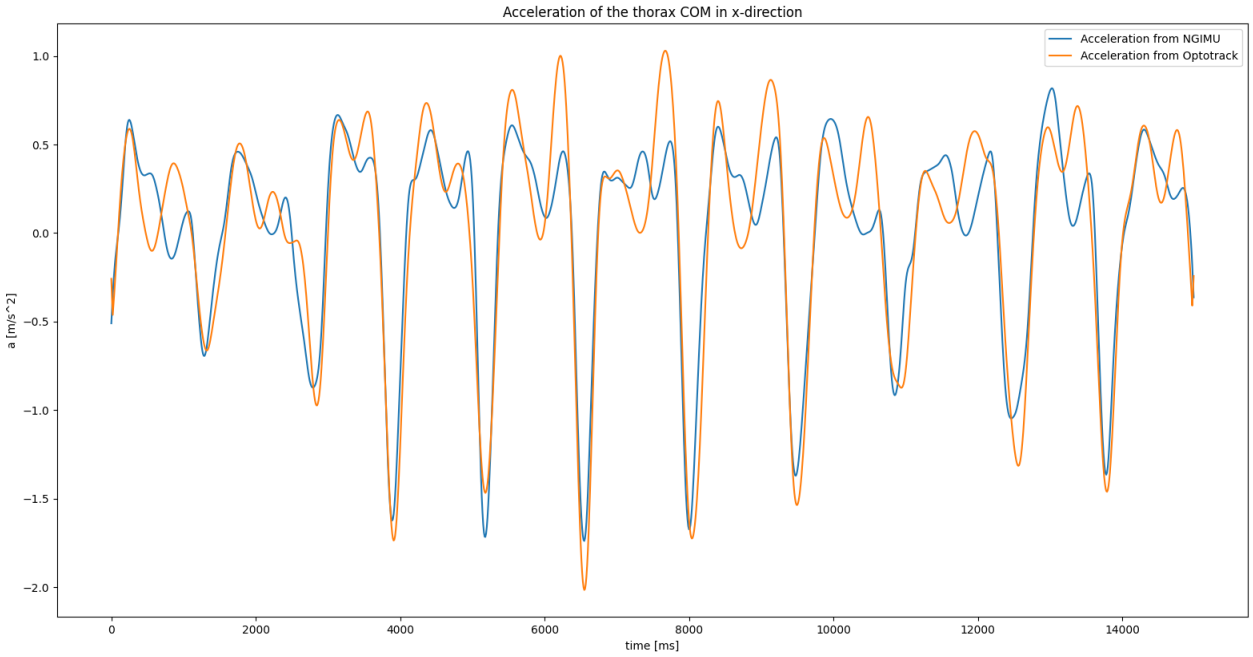

Figure 3: Comparison between measurements of the acceleration of the thorax COM by using the NGIMU and the Optotrack system

3.3.2 Forearm and Upper-arm

Although the simulation model can include the kinematics of the forearm and upper arm in the dynamic model, they have been omitted for this research. Acquiring data kinematic data from the arms during the open-field tests was not feasible. In the treadmill experiment, these data were accumulated, but this research focuses primarily on the rolling resistance in the open-field experiment. Additionally, the effect of the kinematics of the arms is limited compared to the thorax due to their lower mass. To still include the mass of the entire upper body, the mass of the arms, neck and head were added to the mass of the thorax. Furthermore, these body segments were assumed to have the same kinematics as the center of mass of the thorax.

3.3.3 The Reduction Point

The dynamic model of Sauret et al., (Sauret et al., 2013) is used to calculate the rolling resistance. To determine the weight distribution acting on the rear and front wheels, one of the inputs is the force that the thorax exerts on the wheelchair. In the research by Sauret et al. this force is measured using a dynamometer between the seat with feet-rest and the frame of the wheelchair. By measuring the force using this set-up, the location where this force applies is known. This is called the reduction point. However, when calculating this force from the kinematics of the upper body, the location of this reduction point is not known precisely. The wheelchair user can use his lower back, thighs, feet or a combination of these 3 to apply a force to the wheelchair. This can influence the moment balance of the wheelchair and thus the weight distribution and rolling resistance acting on the wheelchair. In this research, the reduction point is assumed to be 25 centimeters directly above the rear wheel axle, as this is the distance from the rear wheel axle to the seat.

3.3.4 Input parameters

As not all properties of this simulation model could be measured directly, some assumptions had to be made. Firstly, the rolling resistance parameters of the front and rear wheels on the surface of the hallway had to be quantified. In the research of Sauret et al. (Sauret et al., 2012), the rolling resistance factor of the rear and caster wheels are estimated for different types of wheel and surfaces using coasting tests. Assuming the surface in the hallway could be categorized as a "hard smooth" surface and the wheels as standard wheels, the rolling resistance parameters can be quantified using the measured wheel radii. This gives rolling resistance parameters of 0.002 and 0.005 for the caster and rear wheels respectively.

Furthermore, the inertial parameters of the separate body segments and wheelchair had to be calculated. The total mass and fore-aft position of the center of mass of the wheelchair could easily be identified using scales. As this research focuses on straight-line wheelchair propulsion and the wheelchair does not tilt or fall over, the wheelchair is assumed to not rotate about any axes. This makes the effect of the moment of inertia about all axes of the wheelchair to be obsolete. The inertial properties of the body segments are estimated using the Zatsiorsky regression equations (Zatsiorky, 1990).

4 Method of Data Collection and Processing

To validate the simulation model constructed in this research, experimental data is required. For this reason, experiments were conducted at the Universitair Medisch Centrum Groningen (UMCG). The main goal of these experiments was to create a complete and adequate data-set to test and validate the simulation model. This data set includes:

1. kinematic data of the forearm, upper arm and thorax
2. kinematic data of the wheelchair
3. force and torque data exerted on the handrim of the wheelchair

4.1 Measurement equipment

To measure kinematic data from the thorax and wheelchair, three Next Generation Inertial Measurement Units (NGIMU's) were used that can be seen in figure 5. The first NGIMU was mounted on the sternum using a strap. Two NGIMU's were fitted on the wheelchair to measure its kinematics: one fixed to the wheel spokes and one fixed below the seat of the wheelchair. The sensors on these NGIMU's include a gyroscope, an accelerometer and a magnetometer that measure at a frequency of 100 Hz (X-ioTechnologies, 2021).

For measuring the forces and torques applied to the handrim, an instrumented wheel Optipush made by Max Mobility (MaxMobility, 2021) was used that can be seen in figure 4. With this instrumented wheel, the triaxial forces which are applied on the handrim are measured in a local coordinate system. Furthermore, the Optipush measures the absolute angle of the wheel and the torque that is applied on the wheel axle. The Optipush system provides measurements at a frequency of 200 Hz (Guo, Kwarciak, Rodriguez, Sarkar, & Richter, 2011).

Figure 4: An Instrumented wheel from Optipush (Guo et al., 2011)

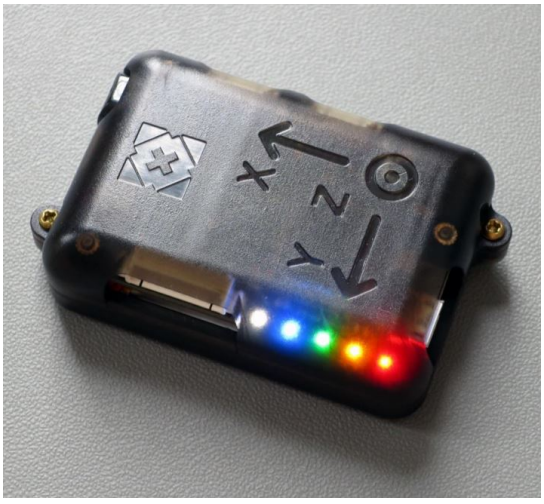

Figure 5: New Generation Inertial Measurement Unit (X-ioTechnologies, 2021)

To gather data on the kinematics of the forearms and upper-arms for the treadmill experiment, the motion tracking set-up of Optotrack was used. Using markers on the specified locations as mentioned in chapter 3.1 and two camera angles, the Optotrack system is able to track the three-dimensional kinematics of the thorax, fore- and upper arms at a frequency of 100 Hz.

4.2 Method of experimenting

Two different experimental set-ups were used to gather data to validate the simulation model of manual wheelchair propulsion: the field-based experiment in the hallway (1) and the treadmill (2). As the Optotrack system uses static cameras to track the kinematic data of fore- and upper-arms, the use of this system was not possible during the hallway tests. This means only the kinematics of the wheelchair and thorax and data from the Optipush could be used as an input for the simulation model in the hall-way experiments. To potentially study the effect of the kinematics of the fore- and upper-arms the treadmill proved to be a useful experimental set-up. Furthermore, this allows for studying the effect of in- or excluding the kinematics of the arms as an input on the results. A complete description of the test protocol can be seen in table 1.

A Manual wheelchair propulsion experiments in the hallway
1. The subject leans forwards and backward 3 times during a standstill for synchronization purposes
2. The subject propels the wheelchair up and down the hallway twice with **free movement** of the **upper body** at:
- Low velocity
- Medium velocity
- High velocity
3. The subject propels the wheelchair up and down the hallway twice at **medium velocity** with the **thorax** in a **fixed position**:
- Straight up
- Leaning forward
- Fully flexed
B Coasting tests in the hallway
1. The wheelchair is pushed by the experimenter and coasts until a standstill twice with the **thorax** in a **fixed position**:
- Straight up
- Fully flexed
2. The wheelchair is pushed by the experimenter and coasts until a standstill twice while the **thorax moves down and up**:
- Slowly
- Quickly
C Treadmill experiments
1. The subject propels the wheelchair for **1 minute** with **free movement** of the **upper body** at:
- Low velocity (1 m/s)
- Medium velocity (1.4 m/s)
- High velocity (1.8 m/s)
2. The subject propels the wheelchair for **1 minute** with the **thorax** in a **fixed position**:
- Straight up (1 m/s)
- Fully flexed (1.4 m/s)

Table 1: Test Protocol for the experiments at the University Medical Center Groningen

4.3 Data Processing

As data from three different sources were gathered, the data first have to be synchronized. Furthermore, the raw data required significant processing before it could be used as a means to validate the simulation model. This data processing is done in Matlab (MATLAB, 2021), with the help of written Matlab functions by M. van Dijk and H.E.J. Veeger (van Dijk, 2021; Veeger, 2021). To compensate for the noise in the raw data, that can result in significant differentiation errors, the input data is filtered with a Butterworth filter with a cut-off frequency of 2 Hz. To synchronize the data from the NGIMU's with the Optipush, the data from both sources on the angular velocity of the rear wheels were used: gyroscopic data from the IMU on the rear wheel spokes (1) and the

differentiated signal of the absolute angle as measured by the Optipush system (2). The results for this can be seen in figure 6 below:

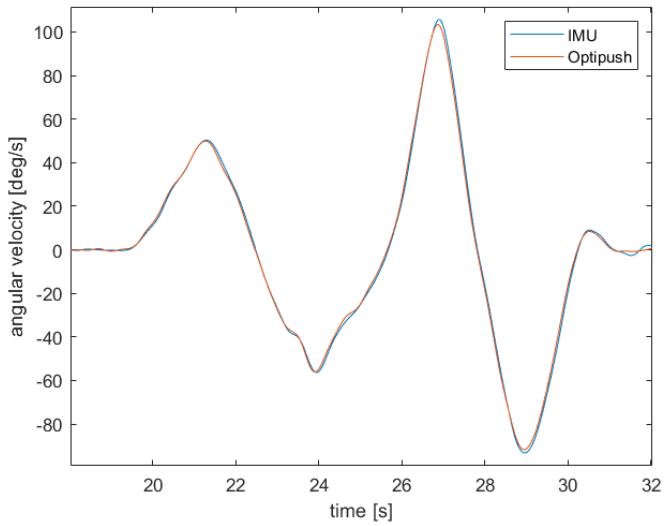

Figure 6: Synchronized angular velocity of the rear wheels as measured by the Optipush wheel and NGIMU during the hallway experiments

After this, the data from the Optotrack system was synchronized with the NGIMU's data for the treadmill experiments. To synchronize the NGIMU data with the Optotrack data, measurements on the velocity of the wheelchair by the NGIMU and Optotrack were used. The gyroscopic data from the IMU on the rear wheel spokes could be used together with the rear wheel radius to determine the velocity. This signal could be compared with the differentiated signal of a measured location on the wheelchair by the Optotrack to synchronize the signals. The synchronized signals can be seen in figure 7 below:

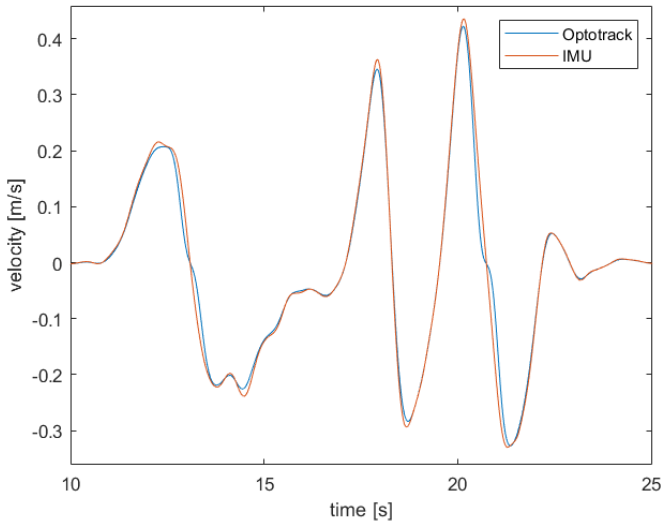

Figure 7: Synchronized linear velocity of the wheelchair as measured by the Optotrack system and NGIMU during a treadmill experiment

4.3.1 Handrim Forces

The handrim forces are measured in the local coordinate system of the Optipush measuring wheel. To know exactly what reaction forces are generated at the hand and forearm due to the pushing of the handrim, the forces are defined in the coordinate system of the wheelchair using the measured wheel angle by the Optipush system. The results for this can be seen in figure 8 below. For clarity purposes, the handrim forces are shown for a period of 35 seconds during the open-field test only.

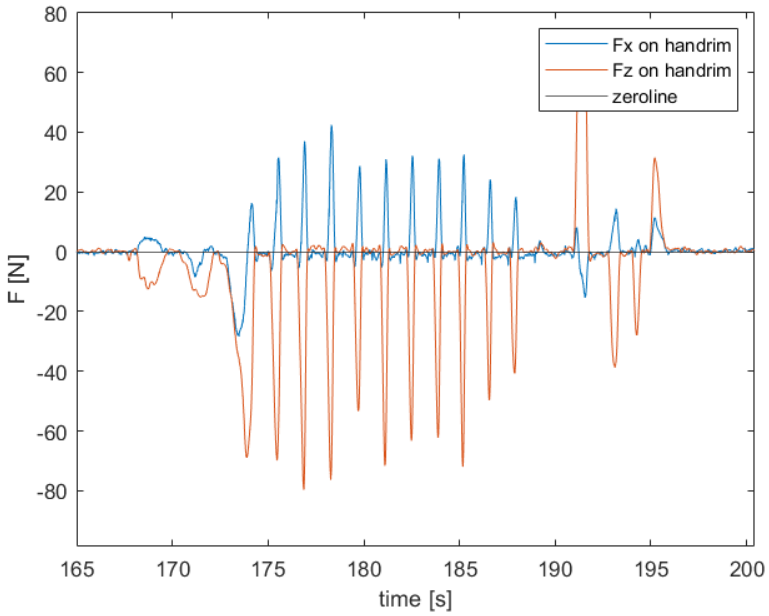

Figure 8: The measured handrim forces by the Optipush measuring wheel in the coordinate system of the wheelchair

5 Results

In this chapter, the results of the open-field experiment will be displayed. Firstly, the results of the coasting tests are shown in chapter 5.1. After this, the results of the test with manual wheelchair propulsion are shown in chapter 5.2. Furthermore, in chapter 5.3, the results of shifting the reduction point (where the force of the thorax is assumed to apply on the wheelchair) are displayed.

5.1 Results of the Coasting Tests in the Open-field Experiment

In this section, the results of the coasting test in the open-field experiment will be shown. The coasting tests allow us to study the workings and results of this simulation model for specific circumstances (i.e. with a fixed thorax position) and without the effect of handrim forces. This can give insights into the workings of a simplified version of this simulation model, before studying the simulation model in more complex situations. During these coasting tests, the experimenter pushes the wheelchair with the test subject on the wheelchair. During the deceleration of the wheelchair, the test subject is instructed to stay in a predetermined pose or perform certain actions. The entirety of the coasting test lasted several minutes and followed the procedure as explained in table 1. As displaying the figures for this complete duration would lead to unclear figures, several periods during this test are highlighted.

5.1.1 Results: Coasting tests with the thorax in the upright position

Firstly, the results of the part of the coasting test in which the test subject is told to keep the thorax in the upright position during deceleration are displayed in figures 9 and 10. In figure 9 the velocity of the wheelchair, thorax angle and the calculated rolling resistance are displayed. Furthermore, the external force that should act on the wheelchair segment to balance the force equation explained in chapter 3.2.1 is shown. As the wheelchair is the last "segment" in the chain, the proximal force acting on the wheelchair should not be present. However, the proximal force in this equation can be seen as an external force acting on this segment. In figure 10, the calculated normal forces acting on the front and rear wheels are displayed.

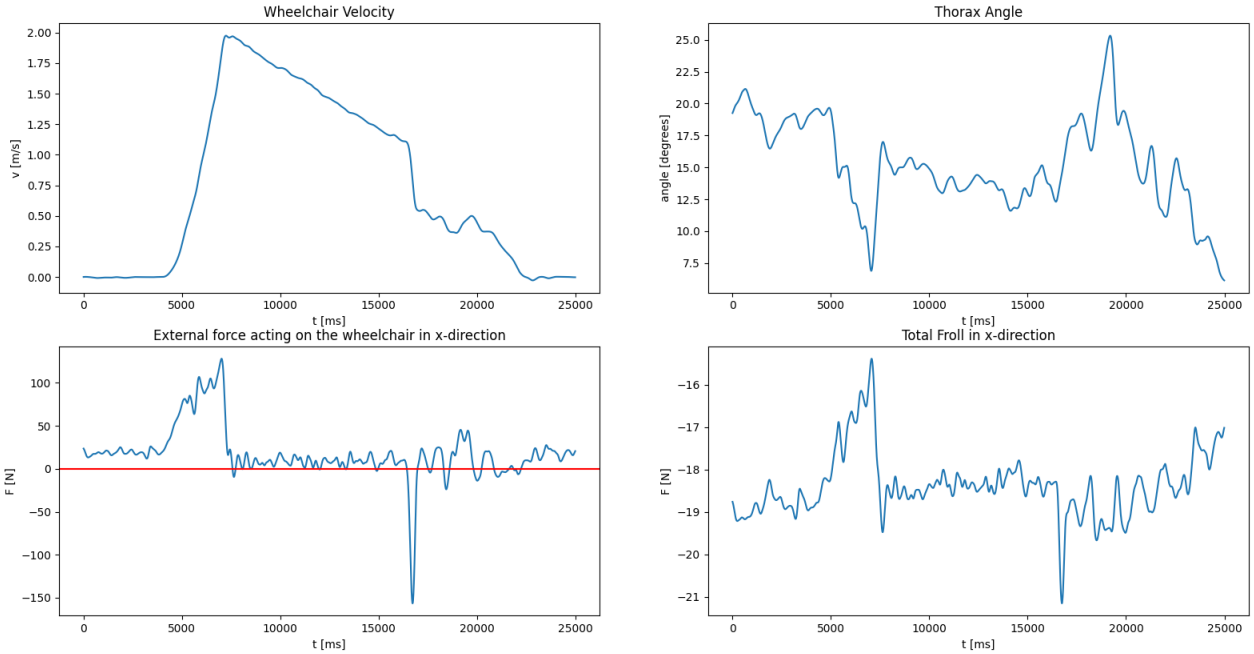

Figure 9: Results of the coasting tests with the thorax in the upright position

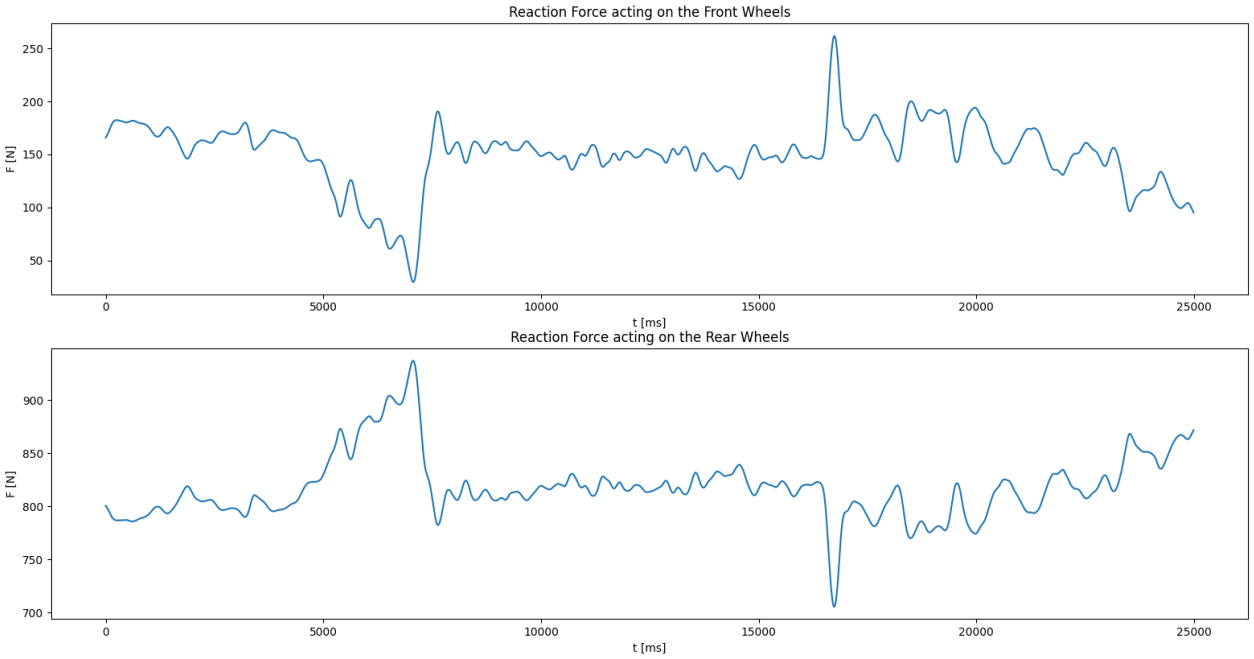

Figure 10: Results of the calculated normal forces acting on the front and rear wheels with the thorax in the upright position

5.1.2 Results: Coasting tests with the thorax in the downward position

The results of the next coasting test are displayed in figures 11 and 12. During this coasting test, the test subject was instructed to keep the thorax in the downward position, resulting in a thorax angle of 70 degrees during coasting.

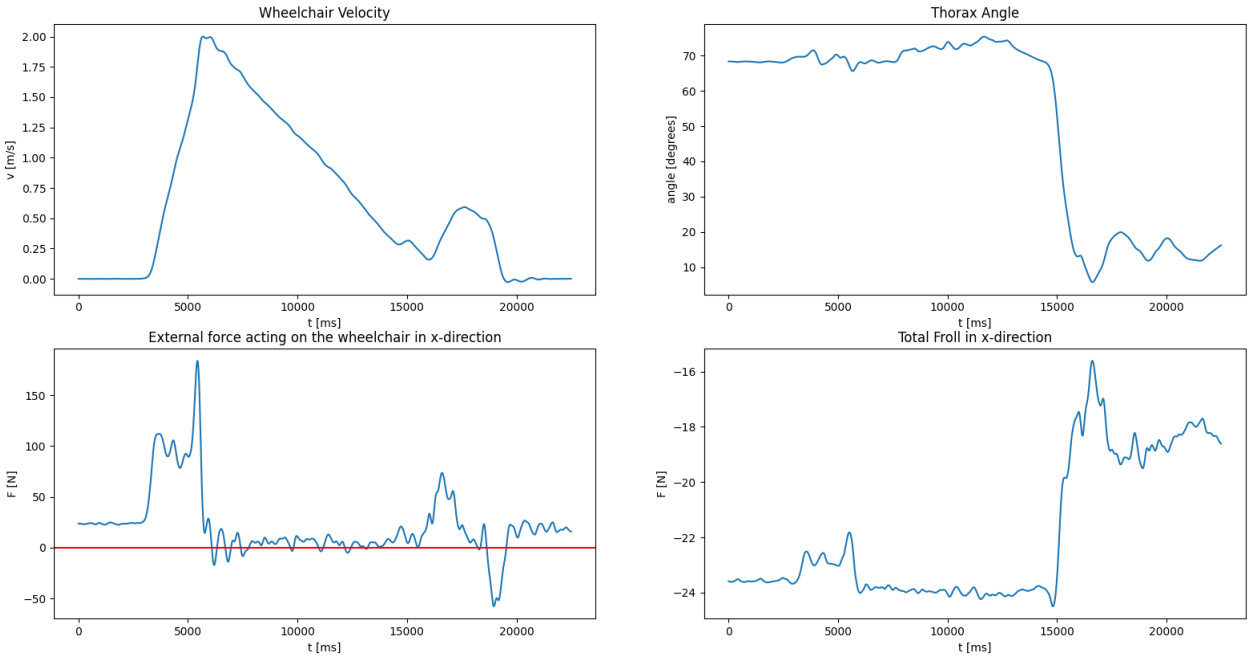

Figure 11: Results of the coasting tests with the thorax in the downward position

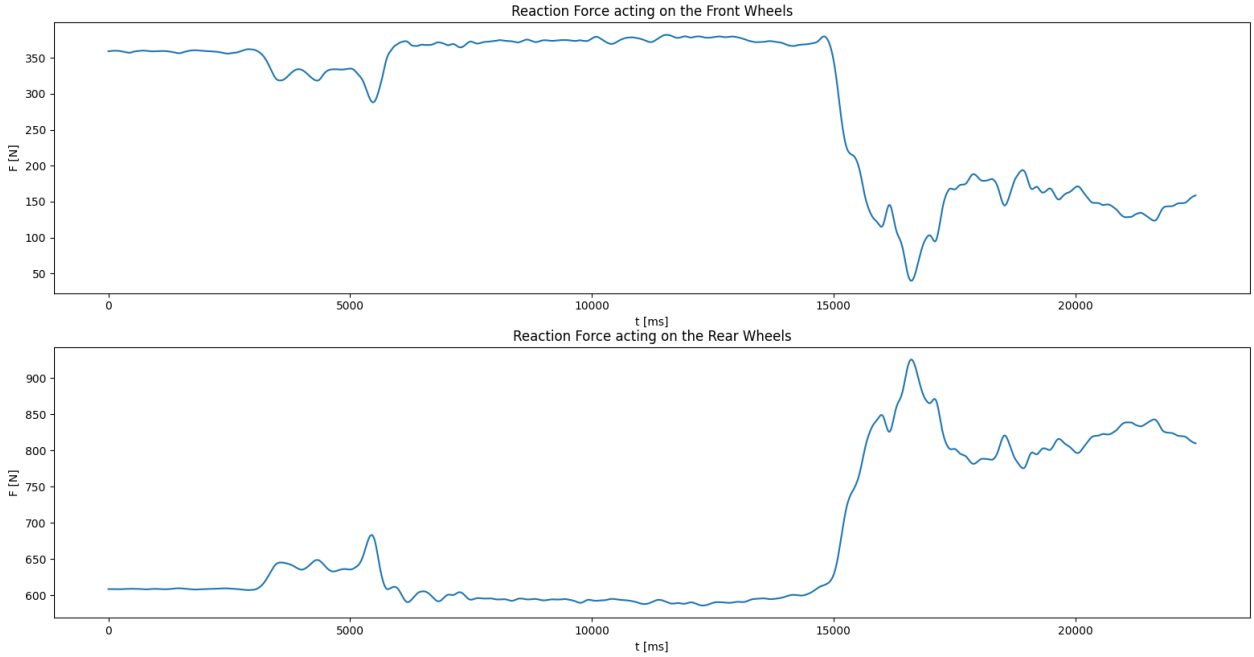

Figure 12: Results of the calculated normal forces acting on the front and rear wheels with the thorax in the downward position

5.1.3 Results: Coasting tests with the changing thorax position

To study the effect of the thorax position and movement further during manual wheelchair propulsion another coasting test was used. In this coasting test, the test subject was instructed to quickly move

its upper body downwards and, after a pause of a couple of seconds, upwards again during coasting as explained in table 1. The result for this can be seen in figures 13 and 14.

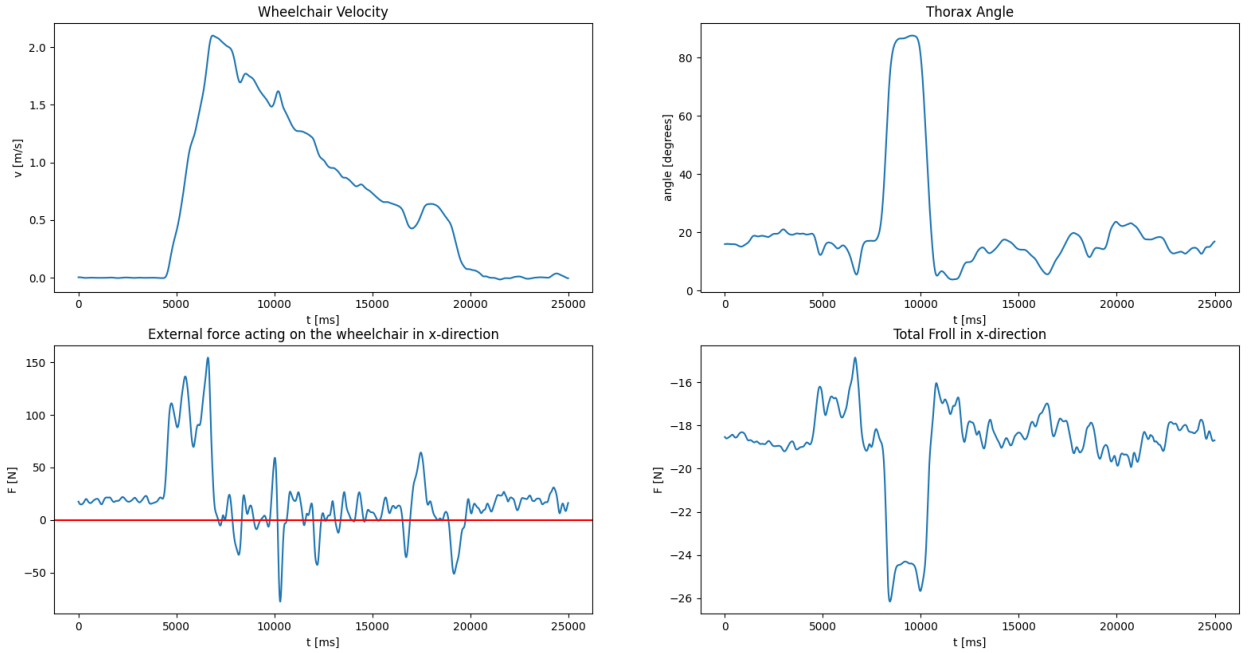

Figure 13: Results of the coasting tests with movement of the thorax

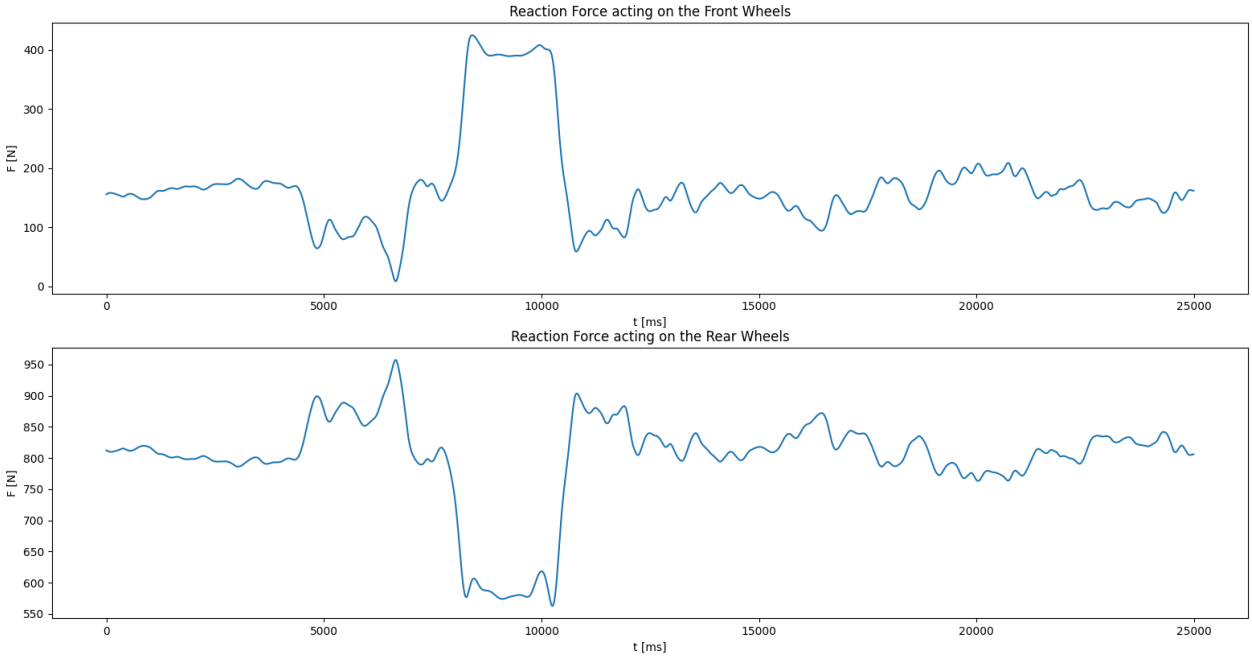

Figure 14: Results of the calculated normal forces acting on the front and rear wheels with movement of the thorax

5.2 Results of the Manual Wheelchair Propulsion Tests in the Open-field experiment

In this chapter, the results of the tests wherein the test-subject manually propels the wheelchair are displayed. Again showing the results over the full duration of the test would lead to unclear figures, so several time periods of this open-field experiment are highlighted.

5.2.1 Results of manual wheelchair propulsion at low speed

Firstly, the results wherein the test subject was instructed to propel the wheelchair at a low speed are showcased in figure 15. In this figure, the velocity of the wheelchair, the thorax angle of the test subject, applied handrim-forces by the test subject and calculated rolling resistance are plotted. During this test, the test subject propelled the wheelchair at a velocity of approximately 1.2 m/s.

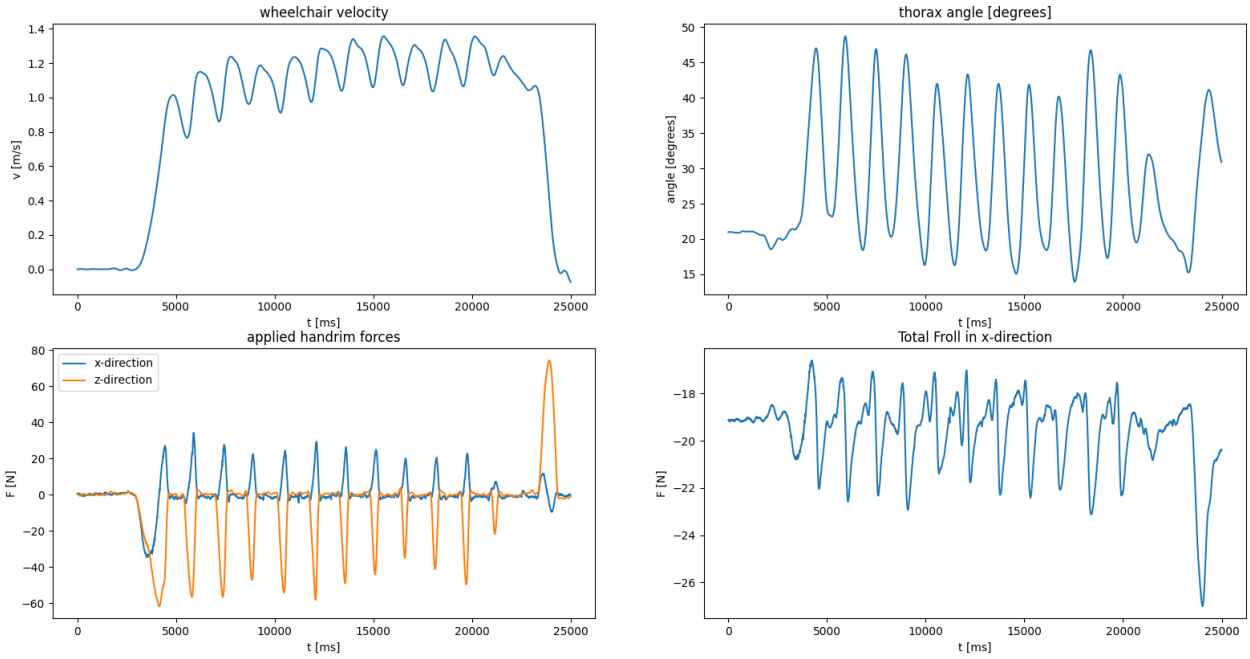

Figure 15: Results of the test with manual wheelchair propulsion at low speed

5.2.2 Results of manual wheelchair propulsion at high speed

During the open-field experiment, the test subject was also instructed to propel the wheelchair at a high velocity. The result for this test can be seen in figure 16. For this particular test, the velocity of the wheelchair exceeded 2.5 m/s at times.

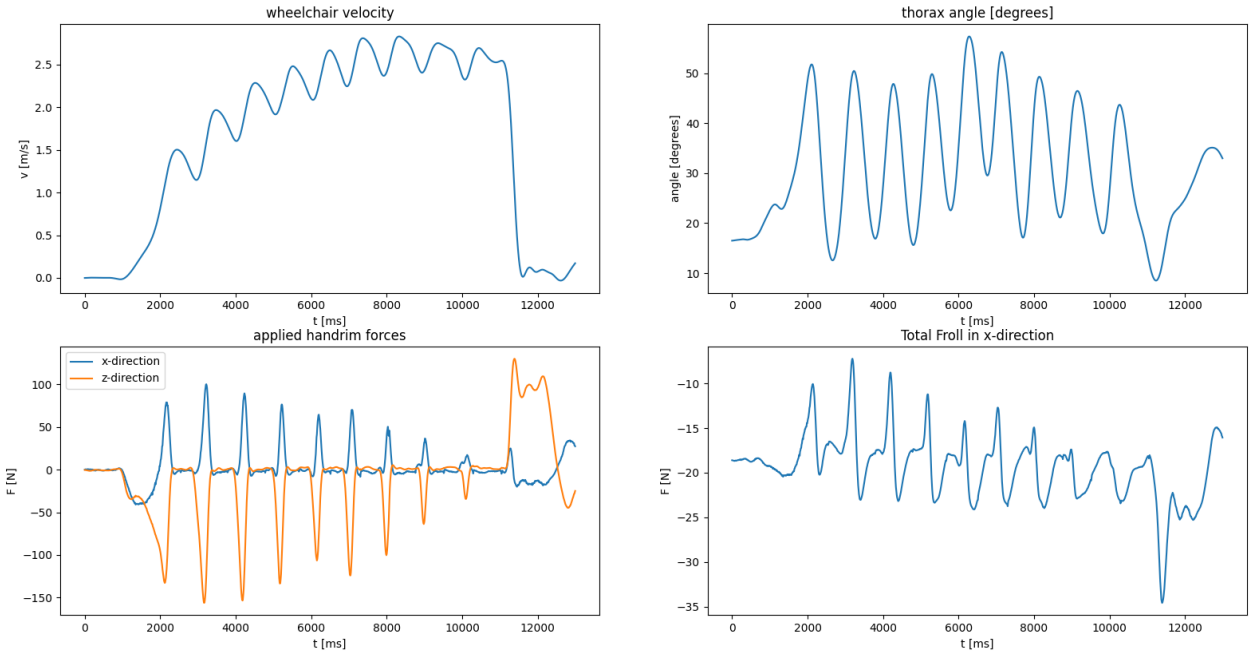

Figure 16: Results of the test with manual wheelchair propulsion at high speed

Figure 17 is used to study the results of the calculated rolling resistance in more in detail, as the results are zoomed in on one stroke of the wheelchair user.

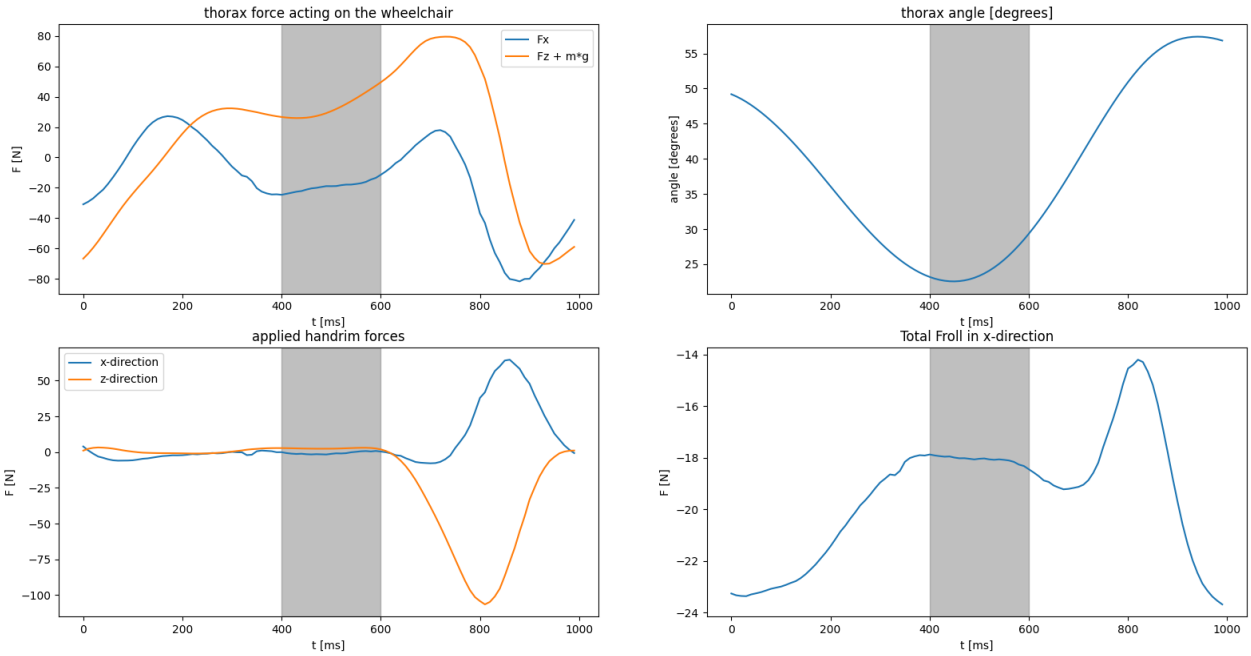

Figure 17: Results of the test with manual wheelchair propulsion at high speed during one stroke

5.3 Results: effect of shifting the reduction point on the calculated rolling resistance

To investigate the effect that the location of the reduction point has on the calculated rolling resistance, the rolling resistance is calculated for different locations of the reduction point. As

explained in chapter 3.3.3, this simulation model assumes that the force that the thorax exerts on the wheelchair applies at this reduction point. The reduction point is initiated at directly 25 centimeters above the wheel axle at the seat of the wheelchair. To investigate the sensitivity of this parameter, this point was shifted forwards and upwards, separately. The results for this are analyzed during a test with wheelchair propulsion at high velocity (2 m/s +). The effect on the maximum and minimum magnitude of the calculated rolling resistance can be seen in table 2. When shifting the reduction point upwards, the effect on the magnitude of the calculated rolling resistance is relatively small. However, shifting the reduction point forwards has a significant impact on the calculated rolling resistance. Shifting the reduction point 0.2 meters forward can lead to an increase of almost 30% in the maximum magnitude of the calculated rolling resistance.

X	Z	max. F	min. F
0	0.45	24.33	5.08
0	0.35	24.16	6.16
0	0.25	24.12	7.23
0.1	0.25	27.72	9.99
0.2	0.25	31.36	12.72

Table 2: The effect of shifting the reduction point forwards and upwards on the magnitude of the rolling resistance

6 Discussion

In this section, the results of the open-field experiment are discussed. Firstly, the results of the coasting tests are discussed in chapter 6.1. After this, the results of the tests with manual wheelchair propulsion are analyzed in chapter 6.2. Lastly, some general remarks on the results are given in chapter 6.3 and limitations of this simulation model are discussed in chapter 6.4.

6.1 Discussion: Coasting tests

The results of the coasting tests with the thorax in an upright position were mostly as expected. During the first seconds when the wheelchair stands still, the external force acting on the wheelchair fluctuates around 20 Newtons, as can be seen in figures 9, 11 and 13. This can be explained by the calculated rolling resistance, which in this case is static friction. In the force equation presented in chapter 3.2.1, the calculated "proximal force" (which in this case is the external force acting on the wheelchair) approximately equals this static friction component. Only when the wheelchair starts to move do we see the effect of the rolling resistance on the kinematics of the wheelchair. When the experimenter pushes the wheelchair to a velocity of approximately 2 meters per second, this push can be seen in the calculated external force acting on the wheelchair. Furthermore, this acceleration pushes the thorax backward into the chair, explaining the decrease in thorax angle clearly visible in figures 9 and 13. This effect is less apparent when the thorax is already in a downward position, as the thorax is then parallel to the direction of the acceleration of the wheelchair.

The mass moment of inertia of the thorax during the push results in a force that the thorax exerts on the wheelchair. As this force applies at a specified distance above the rear wheel axle in this simulation model, this results in a moment about the rear wheel axle. This causes a decrease in the load acting on the caster wheels, which is clearly visible in figures 10, 12, and 14 of the calculated normal forces. A logical consequence is then a decrease in the magnitude of the calculated rolling resistance, which is indeed clearly visible in the results. When the wheelchair abruptly decelerates at the end of the coasting the opposite effect occurs. Furthermore, when the test subject abruptly decelerates the wheelchair, a dip in the calculated external force occurs. This is because the handrim forces were not measured during the coasting tests as these tests were focused on the deceleration of the wheelchair when no forces are applied on the handrim. So as the test subject breaks by grabbing the handrim, this braking force is assumed to be from an external source by the dynamical model.

The results of the coasting tests with the thorax in a downward position are comparable with the tests with the thorax in the upright position. However, there are some key differences. The first obvious difference is the increased deceleration of the wheelchair. As the thorax is tilted forwards during this test (70 degrees vs. 15 degrees with the vertical axis), the load on the front wheels increases compared to the test wherein the test subject held its thorax upright (350 Newtons vs. 150 Newtons). This causes an increase in the rolling resistance acting on the wheelchair, to -24 Newtons from -18 Newtons, hereby explaining the increased deceleration of the wheelchair. At the end of the test, the test subject sits upright again. This decreases the load on the caster wheels, which causes the magnitude of the rolling resistance to decrease.

The results of the coasting tests wherein the thorax moves again look similar to the results of the previous coasting tests. However, when the thorax quickly changes position, notable effects on the results can be distinguished. By quickly tilting the thorax forwards, the thorax accelerates forwards relative to the wheelchair. This pushes the wheelchair backwards, as can be seen in the

velocity plot of the wheelchair. When the thorax moves back into the upright position the opposite effect occurs. Again here the effect of the thorax angle on the calculated rolling resistance is clearly visible, with similar magnitudes for the rolling resistance when the thorax is at rest in the upright and downward positions as compared to the previous coasting tests. However, due to the quick movement of the thorax to reach these thorax positions, additional effects on the rolling resistance can be distinguished. When the thorax reaches the downward position it decelerates. This deceleration of the thorax in the vertical direction increases the total load on the front and rear wheels according to Newton's second law, leading to a peak in the magnitude of the calculated rolling resistance. This also explains why the reaction forces acting on the front and rear wheels do not perfectly mirror each other in figure 14, as the acceleration of the thorax in a vertical direction impacts the sum of the total normal forces acting on the wheels. Subsequently, when the thorax accelerates upwards again, the total load on the wheels again increases, explaining the second peak in the magnitude of the rolling resistance at 10 seconds.

The calculated external forces that should act on the wheelchair to balance the force equation in chapter 3.2.1 fluctuate heavier around the zero-line for the coasting tests wherein the thorax moves than in the previous coasting tests. A potential source for these fluctuations is the uncertainty in the estimated acceleration of the center of mass of the thorax, as explained in chapter 3.3.1. Furthermore, as the open-field experiments do not include measurements of the kinematics of the upper arms and forearms, the mass of the total upper-body is added to the mass of the thorax and is assumed to have the same kinematics. This assumption leads to uncertainty in the force that the thorax applies on the wheelchair. This also has its effect on the calculation of the normal force distribution on the front and rear wheels, as this force influences the balance of moments about the rear wheel axle. The uncertainty of the location of the reduction point, as explained in chapter 3.3.3, also has its effect on the previously mentioned balance of moments.

6.2 Discussion: tests with manual wheelchair propulsion

When studying the complete cycle of the open-field manual wheelchair propulsion, shown in figures 15 and 16, some noteworthy points can be made. Firstly, the different strokes can clearly be distinguished in the calculated rolling resistance. Furthermore, the thorax angle again seems to influence the magnitude of rolling resistance the most, which is to be expected as this increases the load on the caster wheels. However, when looking at the calculated rolling resistance, the thorax angle is certainly not the only factor in determining its magnitude. The magnitude of the applied handrim forces naturally increased during strokes to reach a higher velocity. Furthermore, higher thorax angles were reached during these strokes as larger forces were applied. However, the most significant difference can be seen in the calculated rolling resistance. The pattern in the magnitude of the calculated rolling resistance shows higher peaks and lows when comparing it with the test at low speed. This pattern can be explained by taking a closer look at one stroke cycle in figure 17.

At the start of the first phase of the stroke cycle, the magnitude of the calculated rolling resistance is at its highest. This is logical because the thorax is tilted forwards and the load on the caster wheels is at its peak. Additionally, the thorax accelerates upwards which increases the force that the thorax exerts on the wheelchair and thus increases the total load on the wheels. As the wheelchair user returns its thorax to the upright position, the magnitude of the rolling resistance decreases since the weight distribution shifts backward again. The backward acceleration of the thorax explains the peak in the thorax force acting on the wheelchair in the x-direction. In the rest phase, the rolling resistance stays relatively constant. This is because there are two effects that more or less cancel

out each other in calculating the magnitude of the rolling resistance. Since the thorax accelerates downwards, the total load on the wheels decreases. However, the weight distribution shifts forwards due to the increasing thorax angle. Lastly, the third phase of the stroke cycle begins, wherein the wheelchair user applies the handrim force. As the wheelchair user presses down on the handrim, the force acting on the wheelchair in a vertical direction minus the gravitational force of course reaches its peak. However, the horizontal component of the handrim force has the largest effect on the calculated rolling resistance. The peak in handrim force in x-direction causes the thorax to push the wheelchair back. As this force applies at a distance above the rear wheel axle, this force is an important factor in the moment balance about the rear wheel. Hereby the load on the caster wheels significantly reduces and with that the magnitude of the rolling resistance. At the end of the push when the thorax of the wheelchair user is in the downward position, the magnitude of the rolling resistance is at its highest again due to the shifted weight distribution.

6.3 General Discussion

Overall the results of the simulation model looked promising in describing the relationship between the wheelchair user's action and the calculated rolling resistance. During the propulsion cycle, the fluctuations in the calculated rolling resistance can all be explained by analyzing the kinematics and kinetics of the wheelchair and wheelchair user. The most important factor in determining the magnitude of the rolling resistance appeared to be the trunk angle of the wheelchair user. This can be attributed to the effect the trunk angle has on the weight distribution on the front and rear wheels. This is in accordance with scientific literature, as Brubaker already clearly showed the effect thorax position has on the weight distribution acting on the front and rear wheels (Brubaker et al., 1986). When the weight distribution shifts forwards many studies indeed show a significant increase in rolling resistance (Zepeda, Chan, & Sawatzky, 2016; Sprigle & Huang, 2015; Sauret et al., 2012). Other factors in calculating the rolling resistance can easily be identified in the results of this simulation model and logically be explained. This makes this simulation model a very useful tool to analyze the effect of the wheelchair user's kinematics on the rolling resistance. However, the direct effects of these actions on the rolling resistance have not really been tested in scientific literature, which makes validation of this simulation model a challenge.

6.4 Limitations of this Simulation Model

Some of the results of this research contradict findings in scientific literature. The magnitude of the calculated rolling resistance in this research decreased when the wheelchair accelerated. For example, when the wheelchair was pushed during the coasting tests, the moment of inertia of the thorax caused the weight distribution to shift backward as the thorax was pushed back into the chair. This resulted in a lower magnitude of the calculated rolling resistance as can be seen in figure 9. In scientific literature, the effect of wheelchair acceleration on rolling resistance is seldom studied. However, Teran and Ueda measured an increase in rolling resistance of $8.4N$ for a change in acceleration of the wheelchair of $0.36m/s^2$ (Teran & Ueda, 2017), contradicting the results in this research. Just like in this paper, they argue that the height of the center of mass of the wheelchair user in combination with acceleration and deceleration of the wheelchair can lead to a shift in the weight distribution on the front and rear wheels (Teran & Ueda, 2014). However, in this research, it is argued this can only shift the weight distribution backward. This should result in a lower rolling resistance. A different explanation by Teran and Ueda has to do with the applied torque on the pneumatic tires. When braking and accelerating, the deformation of the

tires will inevitably be higher due to an increase of contact forces at the tire surface. This will lead to an increase in deformation of the tires (and possibly ground), which will lead to increased energy losses due to hysteresis. This could be a possible explanation of the increase in measured rolling resistance by Teran and Ueda. In this simulation model, the terms accounting for this increase in rolling resistance due to an acceleration of the wheelchair are not present. This again highlights the different approaches of this research in determining the rolling resistance compared to other research: calculating the rolling resistance directly from the user's actions and not from the deceleration of the wheelchair.

Furthermore, no increase in rolling resistance can be identified when the velocity of the wheelchair increases in these results. This contradicts multiple studies that show that an increase in wheelchair velocity should result in an increase in rolling resistance (Frank & Abel, 1989; Van der Woude, Geurts, Winkelman, & Veeger, 2003; Teran & Ueda, 2017). This can not be explained by an increased air resistance acting on the wheelchair, influencing the deceleration from which the rolling resistance is estimated, as this was researched mostly on treadmills. When considering the dynamics of this simulation model, the contradicting results of this research make sense. As the velocity of the wheelchair is not a term in the equation to calculate the rolling resistance, it does not influence the magnitude of the calculated rolling resistance. However, from these contradictory results, it must be concluded that some factors contributing to the rolling resistance are not considered in this simulation model. Van der Woude et al. argue this increase in rolling resistance with the increased velocity of the wheelchair has to do with imperfect testing conditions. Again the deformation of the tires will most likely increase at higher velocities due to higher loads acting on the tires. Furthermore, at high velocities, the effect of an imperfect ground surface, imperfect tires or shimmy of the caster wheels on the rolling resistance can become more significant. Again, these terms are not accounted for in the simulation model used in this research.

Additionally, the assumptions and simplifications discussed in chapter 3.3 can significantly impact the calculations of the rolling resistance. The assumption that the force that the thorax exerts on the wheelchair applies at the reduction point might not be completely valid. Firstly, the assumption that this is a static point might not be the case. As the wheelchair user moves in his chair, the wheelchair user exerts a force on the wheelchair. It is impossible to determine to what extent this force is applied by the feet, legs or back using this simulation model. As can be seen in table 2 this can impact the magnitude of the calculated rolling resistance. Especially shifting this reduction point forwards (when the wheelchair user applies relatively more force using his feet for example) affects the calculated rolling resistance heavily. This is because the gravitational force of the upper body then causes a greater moment about the rear wheel axle, which affects the weight distribution. When comparing the load on the caster wheels as a percentage of the total load on the wheels to the results of Sauret et al. some differences arise. In this research, the load distribution on the front wheels varied from approximately 20% to 40% as can be seen in figure 14 (apart from the moment that the wheelchair is pushed by the experimenter). Measurements by Sauret et al. showed a load distribution on the front wheels between 30% and 60% (Sauret et al., 2013). This indicates that shifting the reduction point forwards might lead to more feasible results. However, as this might be very dependent on the type of wheelchair and test subject, this might not necessarily be the case and requires more research. Lastly, the assumptions in determining the acceleration of the center of mass of the thorax and the omission of the forearm and upper arm kinematics could influence the accuracy in calculating the rolling resistance.

7 Conclusion & Recommendations

Rolling resistance is the main resistive force acting on the wheelchair during wheelchair sports. Studying exactly how this rolling resistance is influenced by the wheelchair user's actions could be a useful tool to optimize the movement of wheelchair athletes. However, a simulation model which directly calculates the rolling resistance from the wheelchair user's actions was lacking in scientific literature. This research aimed to fill this research gap by answering the following research question:

How can the rolling resistance be calculated directly from the wheelchair user's kinematics and handrim forces during manual wheelchair propulsion using a segmented inverse kinematic model?

By combining the dynamical model to calculate the rolling resistance from Sauret et al. (Sauret et al., 2013) and the segmented model of Leenen et al. (Leenen et al., 2020) into one simulation model, the rolling resistance can be calculated directly from the wheelchair user's actions. By gathering data on the kinematics and handrim forces of the wheelchair and wheelchair user during coasting and manual wheelchair propulsion experiments, this model could be tested.

7.1 Conclusions

The first results of the calculated rolling resistance look promising. The simulation model behaves as expected during coasting tests and manual propulsion tests. The most important factor in calculating the rolling resistance proved to be the thorax angle, but the effect of other factors such as thorax acceleration and applied handrim forces were also clearly visible in the results. This makes this simulation model a very useful tool to analyze the effect of the wheelchair user's action on the rolling resistance. However, the increase in velocity and acceleration of the wheelchair does not lead to an increase in rolling resistance in this simulation model, contradicting scientific literature. This indicates that some simplifications and assumptions in constructing this simulation model to calculate the rolling resistance affect the validity of this model.

7.2 Recommendations

Additional research to validate the working of the created simulation model is necessary. Firstly, the calculations regarding the acceleration of the center of mass of the thorax need to be tested. Furthermore, the total upper body is seen as one segment with the same kinematics as the thorax in this research, as the influence of the kinematics of the arms on the rolling resistance is deemed to be negligible. By including the kinematics of the upper arms and forearms and comparing the results with the results from this research, the validity of this assumption can be tested. Additionally, researching if the reduction point can be assumed to be a fixed point and, if so, how it can be located might prove to be worthwhile in determining the validity of this simulation model. Lastly, the model can be expanded to work in three dimensions to analyze the rolling resistance of wheelchairs during curvilinear trajectories. This would expand the usability of this simulation model to other wheelchair sports than straight-line wheelchair racing.

References

Bascou, J., Sauret, C., Lavaste, F., & Pillet, H. (2017). Is bearing resistance negligible during wheelchair locomotion? design and validation of a testing device. *Acta of Bioengineering and Biomechanics*, *19*(3).

Brubaker, C. E., et al. (1986). Wheelchair prescription: an analysis of factors that affect mobility and performance. *J Rehabil Res Dev*, *23*(4), 19–26.

Charlton, I. W., & Johnson, G. (2006). A model for the prediction of the forces at the glenohumeral joint. *Proceedings of the Institution of Mechanical Engineers, Part H: Journal of Engineering in Medicine*, *220*(8), 801–812.

De, S. G., Veeger, D., Hollander, A. P., & der Woude Van, L. (2002). Wheelchair propulsion technique and mechanical efficiency after 3 wk of practice. *Medicine and science in sports and exercise*, *34*(5), 756–766.

de Barros Lombardi Jr, A., & Dedini, F. G. (2009). Biomechanical model for the determination of forces on upper-extremity members during standard wheelchair propulsion. *Mathematical and computer modelling*, *49*(7-8), 1288–1294.

Desroches, G., Dumas, R., Pradon, D., Vaslin, P., Lepoutre, F.-X., & Chèze, L. (2010). Upper limb joint dynamics during manual wheelchair propulsion. *Clinical Biomechanics*, *25*(4), 299–306.

Frank, T., & Abel, E. (1989). Measurement of the turning, rolling and obstacle resistance of wheelchair castor wheels. *Journal of biomedical engineering*, *11*(6), 462–466.

Guo, L., Kwarciak, A. M., Rodriguez, R., Sarkar, N., & Richter, W. M. (2011). Validation of a biofeedback system for wheelchair propulsion training. *Rehabilitation Research and Practice*, *2011*.

Harris, C. R., Millman, K. J., van der Walt, S. J., Gommers, R., Virtanen, P., Cournapeau, D., ... Oliphant, T. E. (2020, September). Array programming with NumPy. *Nature*, *585*(7825), 357–362.

Högfors, C., Sigholm, G., & Herberts, P. (1987). Biomechanical model of the human shoulder—i. elements. *Journal of biomechanics*, *20*(2), 157–166.

Hunter, J. D. (2007). Matplotlib: A 2d graphics environment. *Computing in Science & Engineering*, *9*(3), 90–95.

Karlsson, D., & Peterson, B. (1992). Towards a model for force predictions in the human shoulder. *Journal of biomechanics*, *25*(2), 189–199.

Kauzlarich, J., & Thacker, J. (1985). Wheelchair tire rolling resistance and fatigue. *Journal of rehabilitation research and development*, *22*(3), 25–41.

Leary, M., Gruijters, J., Mazur, M., Subic, A., Burton, M., & Fuss, F. (2012). A fundamental model of quasi-static wheelchair biomechanics. *Medical engineering & physics*, *34*(9), 1278–1286.

Leenen, T. A., Trigt, B. V., Hoozemans, M. M., & Veeger, D. H. (2020). Effects of a disturbed kinetic chain in the fastball pitch on elbow kinetics and ball speed. , *49*(1), 67.

MATLAB. (2021). *Matlab (r2020a)*. Natick, Massachusetts: The MathWorks Inc.

MaxMobility. (2021). *The optipush wheel by max mobility.* Retrieved from `http://www.max-mobility.com/`

Morrow, D., Guo, L., Zhao, K. D., Su, F.-C., & An, K. (2003). A 2-d model of wheelchair propulsion. *Disability and rehabilitation*, *25*(4-5), 192–196.

Nikooyan, A. A., Veeger, H., Chadwick, E., Praagman, M., & van der Helm, F. C. (2011). Development of a comprehensive musculoskeletal model of the shoulder and elbow. *Medical & biological engineering & computing*, *49*(12), 1425–1435.

pandas-development team. (2020, February). pandas.

PYTHON. (2021). *Python (3.7)*. Wilmington, Delaware: The Python Software Foundation.

Rodgers, M. M., Tummarakota, S., & Lieh, J. (1998). Three-dimensional dynamic analysis of wheelchair propulsion. *Journal of Applied Biomechanics*, *14*(1), 80–92.

Sauret, C., Bascou, J., de Saint Remy, N., Pillet, H., Vaslin, P., & Lavaste, F. (2012). Assessment of field rolling resistance of manual wheelchairs.

Sauret, C., Vaslin, P., Lavaste, F., de Saint Remy, N., & Cid, M. (2013). Effects of user's actions on rolling resistance and wheelchair stability during handrim wheelchair propulsion in the field. *Medical engineering & physics*, *35*(3), 289–297.

Sprigle, S., & Huang, M. (2015). Impact of mass and weight distribution on manual wheelchair propulsion torque. *Assistive Technology*, *27*(4), 226–235.

Teran, E., & Ueda, J. (2014). Evaluation of wheelchair rolling resistance using a robotic device. In *2014 ieee international workshop on advanced robotics and its social impacts* (pp. 149–154).

Teran, E., & Ueda, J. (2017). Influence of rolling resistance on manual wheelchair dynamics and mechanical efficiency. *International Journal of Intelligent Robotics and Applications*, *1*(1), 55–73.

Van der Helm, F. C. (1994). A finite element musculoskeletal model of the shoulder mechanism. *Journal of biomechanics*, *27*(5), 551–569.

Van der Woude, L., Geurts, C., Winkelman, H., & Veeger, H. (2003). Measurement of wheelchair rolling resistance with a handle bar push technique. *Journal of medical engineering & technology*, *27*(6), 249–258.

van Dijk, M. (2021). *Data analysis functions in matlab python*. TU Delft.

Vanlandewijck, Y., Theisen, D., & Daly, D. (2001). Wheelchair propulsion biomechanics. *Sports medicine*, *31*(5), 339–367.

Veeger, H. (2021). *Data analysis functions in matlab*. TU Delft.

Veeger, H., Van Der Woude, L., & Rozendal, R. (1991). Within-cycle characteristics of the wheelchair push in sprinting on a wheelchair ergometer. *Medicine and science in sports and exercise*, *23*(2), 264.

Virtanen, P., Gommers, R., Oliphant, T. E., Haberland, M., Reddy, T., Cournapeau, D., ... SciPy 1.0 Contributors (2020). SciPy 1.0: Fundamental Algorithms for Scientific Computing in Python. *Nature Methods*, *17*, 261–272.

Warguła, Ł., Wieczorek, B., & Kukla, M. (2019). Determining the rolling resistance coefficient of wheelchairs. *Autobusy: technika, eksploatacja, systemy transportowe*, *20*.

Wheelpower. (2021). Retrieved from `http://www.wheelpower.online/`

Wu, G., Siegler, S., Allard, P., Kirtley, C., Leardini, A., Rosenbaum, D., ... others (2002). Isb recommendation on definitions of joint coordinate system of various joints for the reporting of human joint motion—part i: ankle, hip, and spine. *Journal of biomechanics*, *35*(4), 543–548.

Wu, G., Van der Helm, F. C., Veeger, H. D., Makhsous, M., Van Roy, P., Anglin, C., ... others (2005). Isb recommendation on definitions of joint coordinate systems of various joints for the reporting of human joint motion—part ii: shoulder, elbow, wrist and hand. *Journal of biomechanics*, *38*(5), 981–992.

X-ioTechnologies. (2021). *The next generation imu (ngimu) by x-io technologies.* Retrieved from `https://x-io.co.uk/ngimu/`

Zatsiorky, V. (1990). Methods of determining mass-inertial characteristics of human body segments. In *Contemporary problems of biomechanics* (p. 272–291). Mir.

Zepeda, R., Chan, F., & Sawatzky, B. (2016). The effect of caster wheel diameter and mass distribution on drag forces in manual wheelchairs. *Journal of Rehabilitation Research & Development*, *53*(6).